

## MAGNETORHEOLOGICAL ROTARY BRAKE: ANALYSIS, DESIGN CONSIDERATIONS AND EXPERIMENTAL EVALUATION

B. S a p i ń s k i, S. B y d o ń

Department of Process Control  
AGH – University of Science and Technology

Cracow, Poland

e-mail: deep@agh.edu.pl, e-mail: sbydon@agh.edu.pl

The paper is concerned with analysis, design considerations, construction and experimental testing of a magnetorheological rotary brake (MR brake). Operation principle and basic relationships for the brake are discussed. Magnetic field distribution in the brake is numerically studied using the finite element method (FEM). Structure and materials used in the main components of the brake are described. The brake performance is evaluated via measurement of torque responses.

**Key words:** MR brake, design, magnetic field, construction, experimental testing.

### 1. INTRODUCTION

MR rotary devices are controllable devices operating in the direct-shear mode of MR fluid. This mode can be used to construct brakes, clutches and the like for providing variable torques. Such devices are formed by enclosing MR fluid between the driver and the driven plates (which are in relative rotational motion) and exciting it magnetically, thereby enabling a torque transmission in the applied rotary motion. The initial discovery of MR devices is credited to Jacob Rabinow from the US National Bureau of Standards and refers to his two works concerning the magnetic fluid clutch dated to the late of 1940s (RABINOW [12, 13]).

The controllable MR brake was patented in 1998 (US Patent 5,842,547, [21]). Main benefits of the brake are: simple construction, precise and instantaneous control, easy integration, low voltage and current requirements, high torque at low speed and quiet operation. For this reason the MR brakes are well suited for a variety of applications, two of which are briefly presented below.

For the first time the application of MR brakes for providing controllable forces in exercise machines and in portable devices for rehabilitation of injured limbs was announced by CARLSON [3, 4]. The MR brakes were employed in

these devices as semi-active control elements in cycling and stair-climber types of aerobic exercise machines in conjunction with velocity feedback, wherein the torque is controlled in real time such that the user is forced to maintain a desired target profile. An interesting concept of MR brake application for pneumatic motion control was presented by JOLLY [7]. The Jolly's concept involved placing the MR brake functionally in parallel with pneumatic actuator and that allowed us, through feedback from a position sensor, to achieve accurate and robust motion control. The above applications were based on the MR brake engineered by the research group at Lord Corporation and co-operators. Currently, this company offers the MR brake of MRB-2028 series, being the successor of model MRB-2107-3 (Lord Corporation [20]).

A typical MR brake construction is of a single-disc type in which the rotary plate is rotated while the two casings are fixed. Such construction was also assumed for the MR brake described in this study. The brake was developed for research purposes basing on the patent specification (US Patent 5,842,547, [21]), the available literature (LAMPE *et al.* [8], LEE *et al.* [9], LI and DU [10], HUANG *et al.* [6]) and results of the previous authors research program (SAPIŃSKI and BYDOŃ [14], SAPIŃSKI *et al.* [15]). The main objective of the study was: to explain working principle and basic relationships for the MR brake, to present design considerations and structure of the brake, to characterize materials used for its fabrication, to discuss magnetic field distribution in the brake and to evaluate experimentally its performance.

Note that some other works have been carried out using electrorheological (ER) controllable rotary devices (SEED *et al.* [16], STEVENS *et al.* [17], CARLSON and DUCLOS [2], BULLOUGH [1], PAPADOPOULOS [11], WHITTLE *et al.* [18]). The results concerning the comparison of field-controlled characteristics between MR and ER clutches are provided in (CHOI *et al.* [5]).

## 2. 2. OPERATION PRINCIPLE AND BASIC RELATIONSHIPS

MR brake operates in the direct-shear mode (simply called shear or clutch mode). The MR fluid is sheared by housing surface and rotor surface (see Fig. 1). The MR brake enables continuous control of the torque using external magnetic field. The structure of MR brake is provided in Fig. 2. It enables the gap 6, between housing 7 and rotor 3, to be within the magnetic field 2 produced by coil 1. Rotor is fixed to the shaft 5 which is placed in bearings 4 and can rotate in relation to housing. Wires 9 allow to supply current to the coil. When the magnetic field is applied to the MR fluid 8 inside the MR brake, the characteristics of the fluid increase with practically infinite precision.

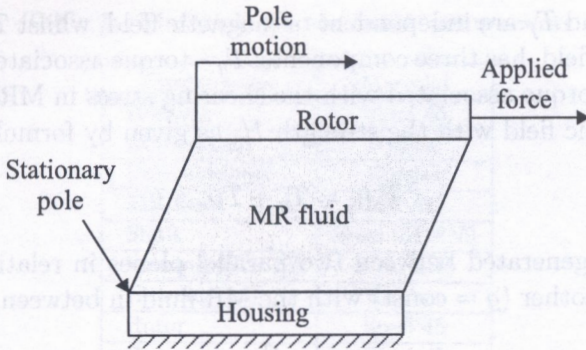


FIG. 1. MR fluid in direct-shear mode.

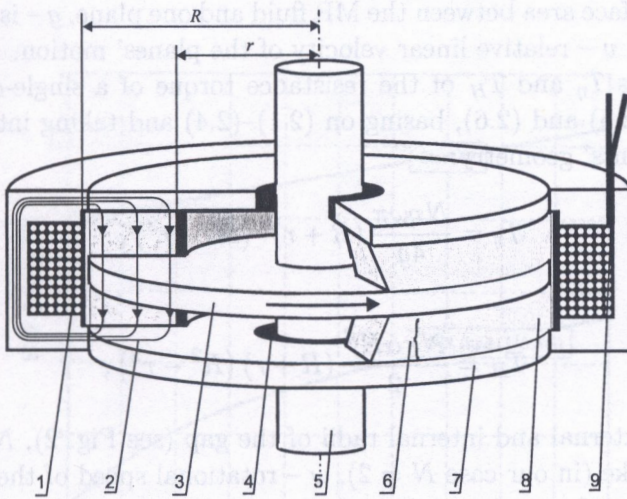


FIG. 2. Diagram of an MR brake.

The shearing stress in an MR fluid under the action of the magnetic field is governed by the Bingham model (CHOI [5]):

$$(2.1) \quad \tau = \eta \dot{\gamma} + \alpha H^\beta$$

where  $\tau$  - shearing stress,  $\eta$  - dynamic viscosity  $\eta = \rho \cdot \nu$  ( $\rho$  - density,  $\nu$  - kinematic viscosity),  $\dot{\gamma}$  - shearing rate,  $H$  - magnetic field strength,  $\alpha, \beta$  - coefficients obtained experimentally.

The MR brake resistance torque  $T$  has three components:

$$(2.2) \quad T = T_i + T_f + T_{MR}$$

where  $T_i$  - torque associated with moment of inertia of mobile components,  $T_f$  - torque of friction in bearings and seals,  $T_{MR}$  - resistance torque of MR fluid.

Torques  $T_i$  and  $T_f$  are independent of magnetic field, whilst  $T_{MR}$ , dependent on the magnetic field, has three components:  $T_\eta$  – torque associated with dynamic viscosity;  $T_H$  – torque associated with the shearing stress in MR fluid under the action of magnetic field with the strength  $H$ , as given by formula:

$$(2.3) \quad T_{MR} = T_\eta + T_H.$$

The force  $F$  generated between two parallel planes in relative motion with respect to one another ( $g = \text{const}$ ) with the MR fluid in between is expressed as:

$$(2.4) \quad F = \frac{\eta \cdot S \cdot v}{g},$$

where  $S$  – interface area between the MR fluid and one plane,  $g$  – distance between the two planes,  $v$  – relative linear velocity of the planes' motion.

Components  $T_\eta$  and  $T_H$  of the resistance torque of a single-disc brake are expressed by (2.5) and (2.6), basing on (2.1)–(2.4) and taking into account the brake components' geometry:

$$(2.5) \quad T_\eta = \frac{N\eta\omega\pi}{4g} (R+r)^2 (R^2 - r^2),$$

$$(2.6) \quad T_H = \frac{N\pi\alpha H^\beta}{2} (R+r) (R^2 - r^2),$$

where  $R, r$  – external and internal radii of the gap (see Fig. 2),  $N$  – number of gaps in the brake (in our case  $N = 2$ ),  $\omega$  – rotational speed of the shaft.

The analysis of experimental results revealed, that the rotational speed of MR brake shaft has not significant influence on resistance torque. This is in agreement with report announced in (CHOI [5]).

### 3. DESIGN CONSIDERATIONS

It is assumed that the designed MR brake should have two active surfaces and a ring-shaped (annular) coil fixed outside, on the rotor circumference. Besides, the range of resistance control should be (0, 4) Nm. The construction materials were selected accordingly and the geometry of brake components was determined.

The magnetic circuit comprises a rotor, housing and MR fluid in the gap (see Fig. 2). The materials specification is provided in Table 1. The magnetisation characteristics for steel 45 and MR fluid 336 AG (Lord Corporation [20]) are shown in Fig. 3. The relationship between the shearing stress and magnetic flux density for the MR fluid is given in Fig. 4.

Table 1. Materials for the brake components.

| Components      | Material     |
|-----------------|--------------|
| Housing         | Steel 45     |
| Coil carcass    | Plastic      |
| Coil windings   | Copper       |
| MR fluid        | 336 AG       |
| Shaft           | Steel 0H18N9 |
| Bearing 6203-ZZ | Steel LH6    |
| Housing seal    | Rubber       |
| Rotor           | Steel 45     |
| Rotor nuts      | Steel 45     |
| Shaft seal      | Rubber       |
| Mounting bolts  | Steel 45     |

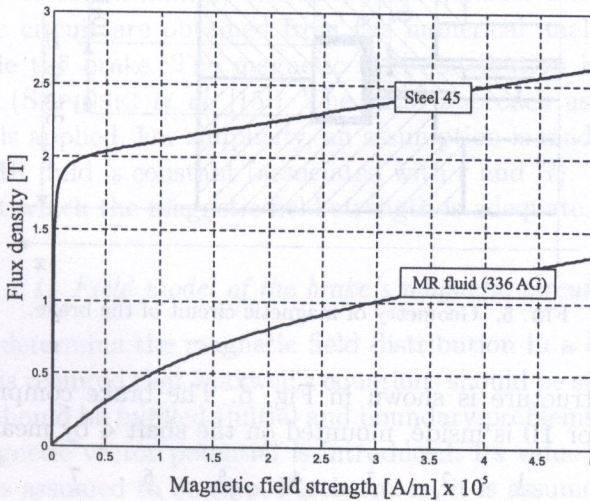


FIG. 3. Magnetic characteristics of the steel and MR fluid used to construct the brake.

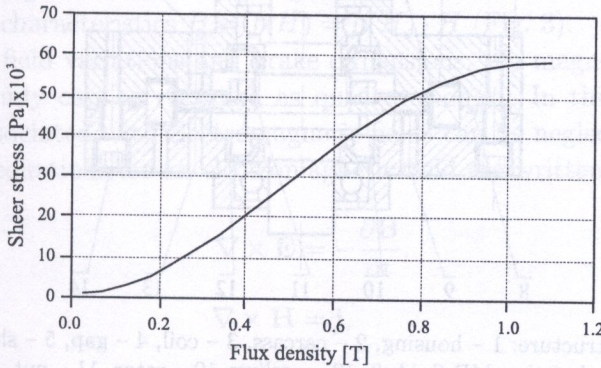


FIG. 4. Shear stress vs. flux density for the MR fluid 336AG.

It is apparent (see Fig. 3 and Fig. 4) that for MR fluid shearing stress control in the range from zero to about  $60 \times 10^3$  Pa, the parameters of the magnetic circuit must be chosen such that the magnetic flux density in the gap should fall in the interval (0, 3) A/m.

Characteristics of brake components' magnetisation (Fig. 3) given in formulas (2.5) and (2.6) would yield the basic rotor and housing dimensions (Fig. 5). The internal radius of the gap is set to be  $r = 24 \times 10^{-3}$  m and the external radius  $R = 32 \times 10^{-3}$  m. The gap height  $g$  is established on the basis of magnetic field distribution.

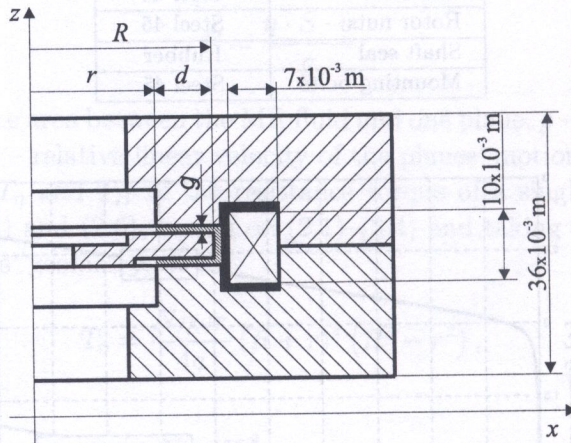


FIG. 5. Geometry of magnetic circuit of the brake.

The brake structure is shown in Fig. 6. The brake comprises a two-part housing 1, a rotor 10 is inside, mounted on the shaft 4 by means of a securing

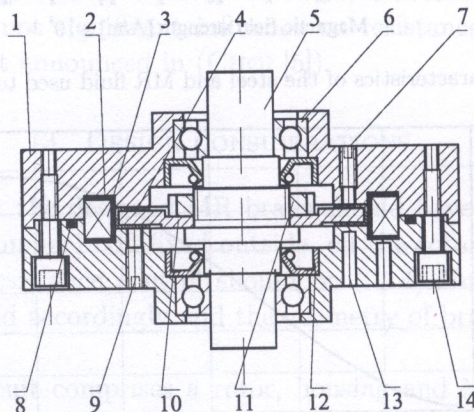


FIG. 6. Brake structure: 1 - housing, 2 - carcass, 3 - coil, 4 - gap, 5 - shaft, 6 - bearing, 7, 9 - openings admitting MR fluid, 8, 12 - sealing, 10 - rotor, 11 - nut, 13 - opening for a temperature sensor, 14 - assembly hole.

nut 11. The shaft is fixed in bearings 6 and the bearing seals and other sealing 12 prevent the leaking of MR fluid and protect the brake inside from impurities. The coil 3 is wound onto the carcass 2 and fixed inside the housing, around the external sections of the rotor. The field generated by the coil activates the MR fluid in the gap 4. There is a seal 8 between the two parts of the housing. The gap is filled with MR fluid through the openings 7 and 9. Additional holes 13 are made for temperature sensors.

#### 4. MAGNETIC FIELD

On account of the axial symmetry of the MR brake, the magnetic field ought to be considered in the plane  $x - z$  where the  $z$ -axis is parallel to the shaft axis while the  $x$ -axis is normal to it (Fig. 5).

The number of coil windings, coil size, wire diameter and the parameters of the magnetic circuit are obtained from the numerical analysis of the magnetic field inside the brake. The magnetic field distribution is obtained using the field model (SAPIŃSKI *et al.* [15]). The FEM approach using the Flux 2D (CEDRAT [19]) is applied. For simplicity, an assumption is made that the width of a gap with MR fluid is constant (associated with  $r$  and  $R$ ). The gap height  $g$  is established at which the magnetic field strength is adequate.

##### 4.1. Field model of the brake's magnetic circuit

In order to determine the magnetic field distribution in a MR brake in the general case, it is required that Maxwell's equations should be solved and boundary conditions should be fulfilled (initial and boundary problems). For simplicity, a notion of magnetic vector potential is introduced. Its value at the boundary of the domain is assumed to be zero. Furthermore, it is assumed that materials for brake's components are isotropic and that the relationship between the field strength and magnetic flux density is given for each material in the form of the magnetisation characteristics  $B = f(H) = \mu(H) \cdot H$  (Fig. 3).

Because of field variations and brake dimensions, the magnetic field considered in this study can be regarded as quasi-stationary. In this case the wave phenomena associated with electromagnetic fields can be neglected.

Maxwell's equations for an electromagnetic field are written as:

$$(4.1) \quad \nabla \times \mathbf{E} = -\frac{\partial \mathbf{B}}{\partial t},$$

$$(4.2) \quad \nabla \times \mathbf{H} = \mathbf{j},$$

$$(4.3) \quad \nabla \cdot \mathbf{B} = 0$$

and

$$(4.4) \quad \mathbf{B} = \mu \mathbf{H},$$

where  $\mathbf{j}$  – density of the forward current,  $\mathbf{E}$  – electric field strength,  $\mathbf{B}$  – magnetic field flux density,  $\mathbf{H}$  – magnetic field strength.

Since  $\nabla \cdot \mathbf{B} = 0$ , the magnetic potential  $\mathbf{A}$  (a vector quantity) is introduced; it is related to magnetic flux density  $\mathbf{B} = \nabla \times \mathbf{A}$ . Hence we get:

$$(4.5) \quad \nabla \times \mathbf{E} = -\frac{\partial(\nabla \times \mathbf{A})}{\partial t},$$

$$(4.6) \quad \nabla \times \left( \frac{1}{\mu} \nabla \times \mathbf{A} \right) = \mathbf{j}.$$

In most magnetic materials the permeability  $\mu$  depends on magnetic field strength  $H$ . In order to determine the distribution of potential  $\mathbf{A}$  it is required that a partial differential equation should be solved for the whole brake volume. In the general case it is given as:

$$(4.7) \quad \frac{1}{\mu(H)} \bar{\nabla}^2 \mathbf{A} = -\mathbf{j} + \gamma \frac{\partial \mathbf{A}}{\partial t},$$

where  $\partial \mathbf{A} / \partial t$  – derivative of magnetic potential with respect to time,  $\mu(H)$ ,  $\gamma$  – magnetic permeability and electrical conductance,  $\mathbf{j}$  – current density in the coil.

Where our considerations are restricted to constant current values, the problem will become that of a magnetostatic field, governed by the partial differential equations:

– for the coil volume:

$$(4.8) \quad \frac{1}{\mu(H)} \bar{\nabla}^2 \mathbf{A} = -\mathbf{j},$$

– for the remaining elements:

$$(4.9) \quad \bar{\nabla}^2 \mathbf{A} = 0.$$

On account of the brake's cylindrical symmetry, the vector potential and current should have one component only:  $\varphi$ . That enables 2D computations in the cylindrical coordinate system  $x - z$ :

$$(4.10) \quad E_\varphi = -\frac{\partial A_\varphi}{\partial t}$$

and hence:

$$(4.11) \quad \frac{1}{\mu(H)} \nabla^2 A_\varphi = -j_\varphi,$$

$$(4.12) \quad \nabla^2 A_\varphi = 0.$$

Given the vector potential  $\mathbf{A}$ , the magnetic flux density distribution is obtained:

$$(4.13) \quad \mathbf{B} = \nabla x \mathbf{A}.$$

Following the field model formulation, the numerical analysis of the magnetic field distribution in the brake was performed. Selected results are shown in Figs. 7–9.

#### 4.2. Field distribution

Figure 7 shows the magnetic flux density distribution halfway up the gap with the parameters  $g = (0.3, 0.5, 0.7, 0.9) \times 10^{-3}$  m for the constant level of applied current. The gap width  $g = 0.5 \times 10^{-3}$  m. Figure 8 shows the flux density distribution halfway up the gap height for various levels of the applied current (gap width  $g = 0.5 \times 10^{-3}$  m). It is apparent that homogeneous distribution is obtained for the gap length  $6 \times 10^{-3}$  m. Figure 9 shows magnetic field distribution in the brake, for same gap width ( $g = 0.5 \times 10^{-3}$  m), for the applied current 0.3 A.

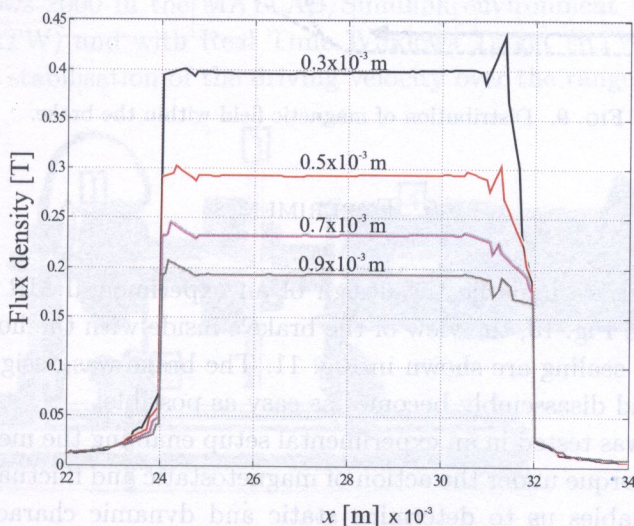


FIG. 7. Flux density distribution along the gap for various gap sizes.

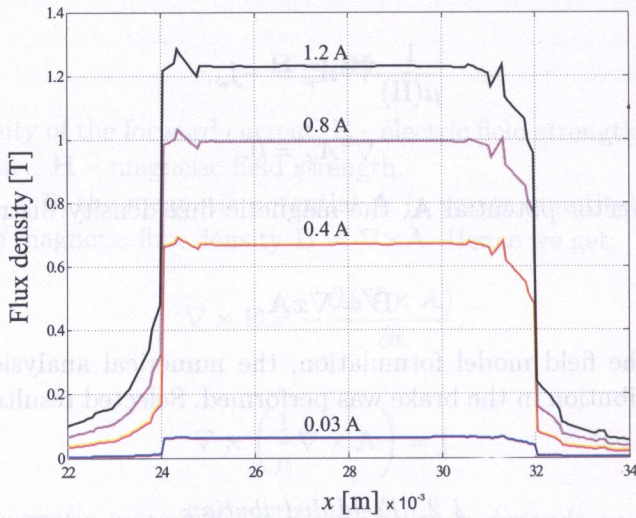


FIG. 8. Flux density distribution along the gap for various current levels.

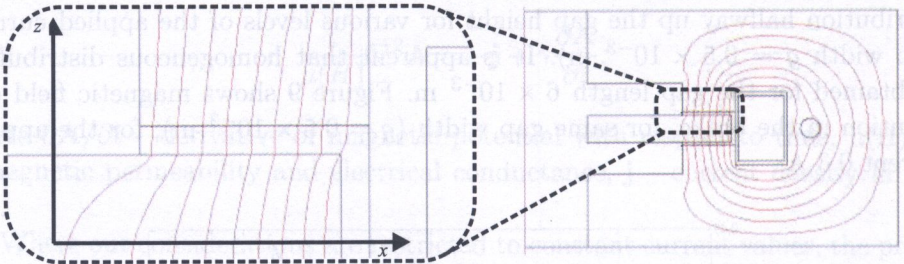


FIG. 9. Distribution of magnetic field within the brake.

## 5. EXPERIMENTS

These objectives underlie the design of an experimental MR brake, shown schematically in Fig. 10, the view of the brake's inside with the housing section, fixed rotor and sealing are shown in Fig. 11. The brake was designed such that its assembly and disassembly becomes as easy as possible.

The brake was tested in an experimental setup enabling the measurements of the resistance torque under the action of magnetostatic and fluctuating magnetic fields. That enables us to determine static and dynamic characteristics. The amplifying factor was established, too.

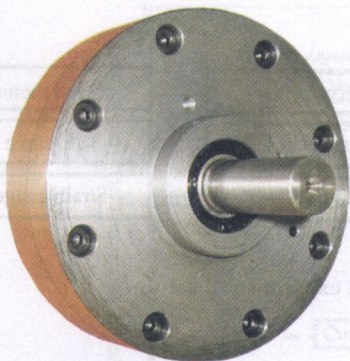


FIG. 10. General view of the brake.

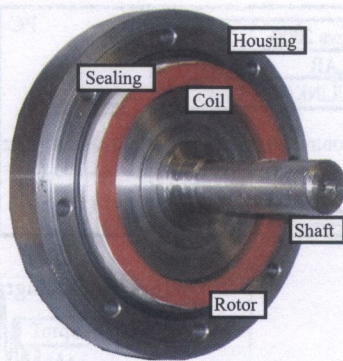


FIG. 11. Inside view of the brake.

### 5.1. Experimental setup

The general view of the experimental setup is shown in Fig. 12, while the block diagram in Fig. 13. The mechanical components of the setup are the driving unit comprising a servo-motor **5** and a planetary gearbox **4**. On the transmission shaft is a rigid clutch **3** of a large moment of inertia. The clutch connects the drive unit with the MR brake **1** shaft and the impacts of abrupt MR brake torque changes on the driving unit can be thus minimised. Strain gauge **2** was used to measure the resistant torque. The electric components of the setup are: a PC with a multi I/O board of RT-DAC4 series, a servo-drive, a MR brake drive, a torque measurement circuit and a coil current measurement circuit. The PC operates under Windows 2000 in the MATLAB/Simulink environment with Real Time Workshop (RTW) and with Real Time Windows Target (RTWT). The servo-drive enables stabilisation of the driving velocity over the range (0, 100) rad/s.

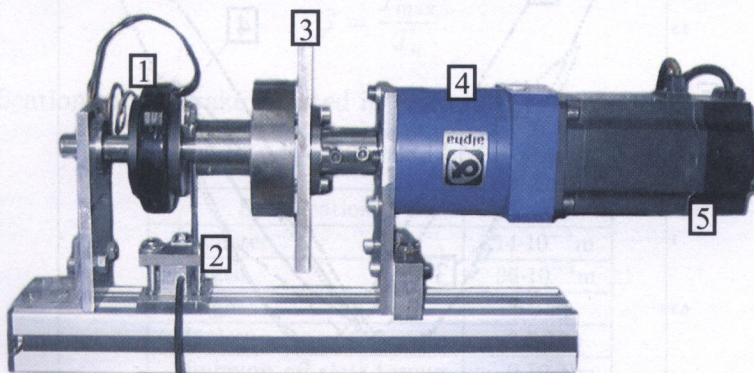


FIG. 12. Experimental setup: 1 – MR brake, 2 – strain gauge, 3 – rigid clutch, 4 – planetary gearbox, 5 – servomotor.

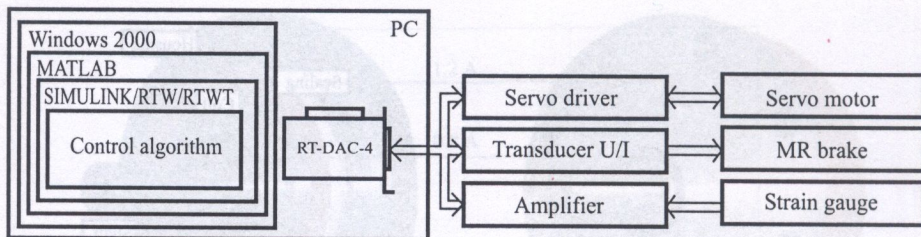


FIG. 13. Block diagram of the experimental setup.

The signal of the brake resistant torque is measured using a strain gauge and then is amplified in an instrumental amplifier. The electronic circuit of an amplifier controlling the coil voltage is also used for measuring the current levels in the coil.

### 5.2. Torque responses

Torque responses were measured with a strain gauge placed by the brake's shaft rotating at 100 rad/s. At the same time measurements were taken of voltage and current in the coil. Measurement data were then processed to yield the static and dynamic characteristics of the brake (Figs. 14 and 15). Dynamic characteristics are given as plots of current vs. torque for the step-like variations of voltage across the coil clamps  $u(t) = A \cdot 1(t)$ .

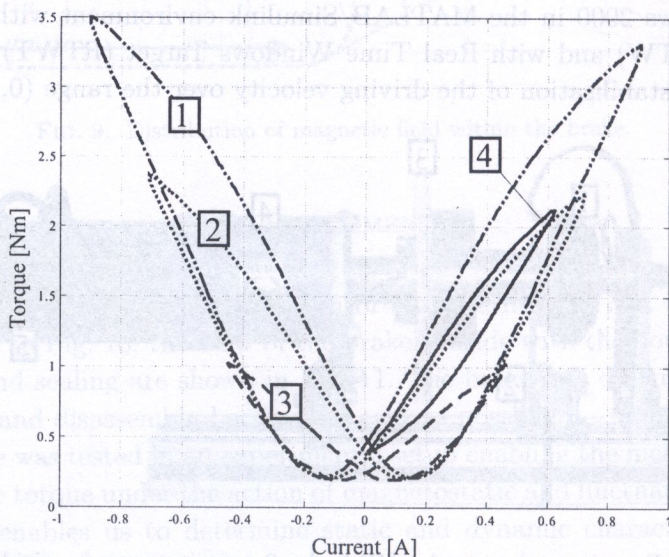


FIG. 14. Torque vs. current under the action of magnetostatic fields.

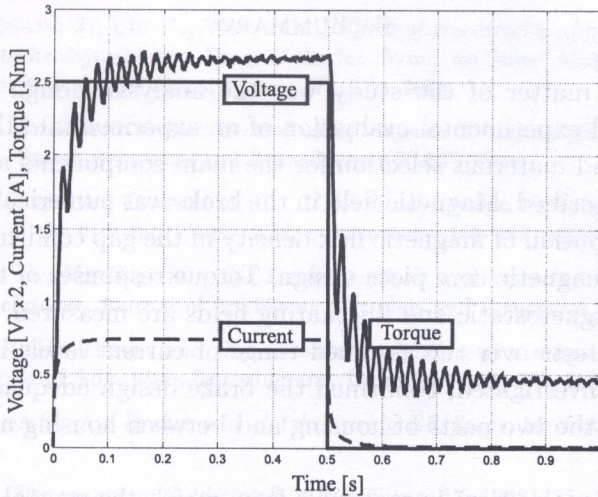


FIG. 15. Current and torque responses to step voltage input for  $A = 5$  V.

Actual shape of static characteristics reveals the effects of magnetic hysteresis. The curves 1, 2, 3 in Fig. 14 were obtained for the bipolar supply voltage, while the curve 4 for the unipolar supply voltage.

Tests reveal that the changes of the resistance torque cannot be completely utilised when the coil supply system is unipolar, due to the presence of residual magnetism.

For the engineered brake we have determined also the amplifying factor  $G$  (see Table 2). This factor represents the ratio of the maximal resistance torque  $T_{\max}$  (maximal current level) to the resistance torque  $T_o$  (no current in the coil):

$$(5.1) \quad G = \frac{T_{\max}}{T_o}.$$

Specification of the brake is listed in Table 2.

Table 2. Specification of the brake.

| Specification                   | Value                 |
|---------------------------------|-----------------------|
| Diameter                        | $114 \cdot 10^{-3}$ m |
| Length                          | $36 \cdot 10^{-3}$ m  |
| Weight                          | 2.1 kg                |
| Maximum <i>on-state</i> torque  | 3.5 Nm                |
| Minimum <i>off-state</i> torque | 0.19 Nm               |
| Maximum current                 | 0.9 A                 |
| Coil resistance                 | 6.6 $\Omega$          |
| Amplifying factor $G$           | 18.4                  |

## 6. SUMMARY

The subject matter of the study was the analysis, design considerations, construction and experimental evaluation of an experimental MR rotary brake. Dimensioning and materials selection for the main components and structure of the brake are described. Magnetic field in the brake was numerically studied. The computed distribution of magnetic flux density in the gap confirms the adequacy of the adopted magnetic core piece design. Torque responses of the brake under the action of magnetostatic and fluctuating fields are measured.

Preliminary tests over the assumed range of current levels in which torque responses were investigated, confirmed the brake design adequacy. The applied sealing between the two parts of housing and between housing and shaft proves to be effective.

The residual magnetism in materials from which the control circuit is made gives rise to the errors due to ambiguous characteristics, approaching 30% in the case of bipolar control and 15% when unipolar control of the coil current is executed. Such high error values render the torque control a really formidable task.

While compared to conventional solutions, the engineered brake has a simple design and a small number of components (there are no mobile control elements).

Research is now under way to improve the brake design, with the main focus on optimisation of its magnetic circuit.

## ACKNOWLEDGMENT

This work has been supported by AGH – University of Science and Technology under research programme no. 10.10.130.213/2005.

## REFERENCES

1. BULLOUGH W. A., *The ER clutch: design, performance, considerations and operation*, Proc. of IMechE, **207**, 253–266, 1993.
2. CARLSON J. D., DUCLOS D. G., *ER fluids clutches and brakes: fluid properties and mechanical considerations*, Proc. of the 2-nd Int. Conf. on ER Fluids, 353–367, 1992.
3. CARLSON J. D., *Magnetorheological fluid devices and process controlling force in exercise equipment utilizing same*, U.S. Patent no: 5,816,372, 1994.
4. CARLSON J. D., *Portable controllable fluid rehabilitation devices*, U.S. Patent no: 5,711,746, 1998.
5. CHOI S. B., HONG S. R., CHEONG C. C., *Comparison of field-controlled characteristics between ER and MR clutches*, Journal of Intelligent Material Systems and Structures, **10**, 615–619, 1999.

6. HUANG J., ZHANG J., LIU N., WANG CH., *Effect of eccentricity of properties of a cylindrical magnetorheological brake*, Proc. of the Int. Symp. on Smart Materials for Engineering and Biomedical Applications, China, 371–374, 2004.
7. JOLLY M. R. *Pneumatic motion control using magnetorheological fluid technology*, 27-th Int. Symp. on Smart Actuators and Transducers (ICAT) 1999.
8. LAMPE D., THESS A., DOTZAUER C., *MRF clutch: design considerations and performance*, Proc. of the 6-th Int. Conf. on New Actuators, 449–452, 1998.
9. LEE U., KIM D., HR N., JEON D., *Design analysis and experimental evaluation of an ER and MR clutches*, Journal of Intelligent Materials and Structures, **10**, 701–707, 1999.
10. LI W. H., DU H., *Design and Experimental evaluation of a magnetorheological brake*, The Int. Journal of Adv. Manufacturing and Technology, **21**, 508–515, 2003.
11. PAPADOPOULOS C. A., *Brakes and clutches using ER fluids*, Mechatronics, **8**, 641–669, 1998.
12. RABINOW J., *The magnetic fluid clutch*, AIEE Trans. **67**, 13081315, 1948.
13. RABINOW J., *Magnetic fluid clutch*, National Bureau of Standards Technical News Bulletin, **32**, 4, 54–60, 1948.
14. SAPIŃSKI B., BYDOŃ S., *Characteristics for a magnetorheological rotary brake – experimental investigation*, Proc. of Int. Carpathian Control Conf., 373–378, 2004.
15. SAPIŃSKI B., BYDOŃ S., JARACZEWSKI M., *Magnetic field in a rotary brake with a magnetorheological fluid* [in Polish], Czasopismo Techniczne Politechniki Krakowskiej, z. 5-M, 325–333, 2004.
16. SEED M., HOBSON G. S., *Voltage-controlled electrorheological brake*, Proc. of the IASTED Int. Symp. on Measurements, Processes and Control, Italy, 280–284, 1986.
17. STEVENS N. G., SPRONSTON J. L., STANWAY R., *An experimental study of electro-rheological torque transmission*, ASME Journal: Mechanisms, Transmissions and Automation in Design, 182–188, 1988.
18. WHITTLE M., ATKIN R. J., BULLOUGH W. A., *Dynamics of a radial electrorheological clutch*, Journal of Modern Physics, **13**, 2119–2126, 1999.
19. CEDRAT, User's guide FLUX 3D, France 2000.
20. LORD CORPORATION, <http://www.rheonetic.com> 2003.
21. US PATENT 5,842,547, Controllable brake, 1998.

Received June 13, 2005.